Rationalizing strain engineering effects in rare-earth nickelates

F. Y. Bruno,[1] K. Z. Rushchanskii,[2] S. Valencia,[3] Y. Dumont,[4] C. Carrétéro,[1] E. Jacquet,[1] R. Abrudan,[3,5] S. Blügel,[2] M. Ležaić,[2] M. Bibes,[1] and A. Barthélémy[1]

[1]*Unité Mixte de Physique CNRS/Thales, Campus de l'Ecole Polytechnique, 1 Avenue A. Fresnel, 91767 Palaiseau, France and Université Paris-Sud 11, 91405 Orsay, France*

[2]*Peter Grünberg Institut, Quanten-Theorie der Materialien, Forschungszentrum Jülich and JARA, 52425 Jülich, Germany*

[3]*Helmholtz-Zentrum-Berlin für Materialen und Energie, Albert-Einstein-Strasse 15, 12489 Berlin, Germany*

[4]*Groupe d'Etude de la Matière Condensée, Université de Versailles St-Quentin en Yvelines/CNRS, 45 avenue des Etats-Unis, 78035 Versailles, France*

[5]*Institut für Experimentalphysik/Festkörperphysik, Ruhr-Universität Bochum, 44780 Bochum, Germany*

(Received 21 June 2013; revised manuscript received 30 August 2013; published 5 November 2013)

The physics of nickel perovskites is rich with various competing electronic phases that can be tuned by chemical or external degrees of freedom. As such, nickelates show strong potential for oxide electronics devices based on strongly correlated systems. However, their complexity has hitherto challenged a detailed understanding of classical material engineering effects using, e.g., epitaxial strain. Here we investigate this important pending issue by comparing experimental data with results from first-principles calculations using the Heyd-Scuseria-Ernzerhof hybrid exchange-correlation functional. The theory properly describes the magnetic ground state as well as the preferred orbital occupation observed by x-ray linear dichroism. It also shows that the strain-induced modulation of the metal-to-insulator transition temperature is likely driven by changes in the bandwidth, rather than by the charge-transfer energy.

DOI: 10.1103/PhysRevB.88.195108 PACS number(s): 71.27.+a, 31.15.V−, 75.47.Lx

Nickel perovskites $R\mathrm{NiO_3}$ (where R is a rare earth from Pr to Lu) display a sharp metal-insulator (MI) transition driven by strong electron correlations.[1–4] The low-temperature insulating state is characterized by the appearance of two nonequivalent Ni sites with different oxygen surroundings,[5] possibly accompanied by charge disproportionation effects.[5,6] In addition, nickelates exhibit a transition from a paramagnetic phase to an antiferromagnetic phase occurring at the Néel temperature (T_N) $\leqslant T_{\mathrm{MI}}$.

Advances in epitaxy techniques have recently made possible the growth of coherently strained oxide thin films, and strain engineering has emerged as a powerful tool to unveil novel electronic phases. The discovery of ferroelectricity in coherently grown thin films of $\mathrm{SrTiO_3}$[7] and $\mathrm{EuTiO_3}$,[8] the prediction of multiferroicity in Bi-based double perovskites,[9] and the stabilization of magnetic orders in thin films of $\mathrm{BiFeO_3}$[10] not present in the bulk are some remarkable examples. Heterostructures comprising fully strained $R\mathrm{NiO_3}$ thin films have also attracted a lot of attention. This interest is driven by the observation of phase transitions controlled by dimensionality[11] and the very exciting predictions of superconductivity,[12] topological phases,[13] and multiferroicity[14] in nickelate-based heterostructures. Moreover, the integration of $\mathrm{SmNiO_3}$ thin films onto Si was recently demonstrated, which constitutes an important step towards applications.[15]

Despite the excitement regarding $R\mathrm{NiO_3}$ films, the basic aspects of the influence of epitaxial strain on their properties are yet not fully understood. In the bulk, applying hydrostatic pressure produces the same effect as increasing the R-site ionic radii, which decreases T_{MI} as a consequence of the increased one-electron bandwidth determined by the Ni-O-Ni bond angle.[2,16,17] In films, epitaxial strain—by nature anisotropic—has a more complex influence. Experimentally, contradictory results have been obtained, with reports, for instance, in $\mathrm{NdNiO_3}$ films of either an increase,[18] or a decrease[19] of T_{MI}, or a suppression of the insulating state[20] induced by compressive strain. In the same material, tensile strain was found to lower T_{MI},[19] but also to suppress the transition for strain values larger than 1%–2%.

This body of conflicting results motivates our reinvestigation of the influence of epitaxial strain on $R\mathrm{NiO_3}$ films, in order to discriminate between extrinsic effects (related to the appearance of defects such as oxygen vacancies, cationic deficiency, etc.) and intrinsic factors. In the latter case, it has been argued that T_{MI} is determined by strain-induced changes in the charge-transfer energy.[21] In the present paper, through a joint experimental and theoretical study of strain effects on $\mathrm{SmNiO_3}$ (SNO) thin films, we hope to clarify these pending issues.

In the bulk, SNO exhibits a $T_{\mathrm{MI}} = 400$ K and a Néel temperature $T_{\mathrm{N}} = 220$ K. The room-temperature lattice parameters of SNO are $a = 5.33$ Å, $b = 5.43$ Å, and $c = 7.56$ Å, or in pseudocubic notation $a_p = 3.796$ Å.[22] To limit the possible formation of strain-induced structural defects, we restricted ourselves to moderate strain levels by growing films on $\mathrm{SrLaAlO_4}$ (SLAO), $\mathrm{LaAlO_3}$ (LAO), and $\mathrm{SrLaGaO_4}$ (SLGO) substrates that impose compressive (–1%), virtually zero (–0.3%), and tensile (1.2%) strain, respectively. We grew films from 5 up to 60 unit cells (u.c.) thick using pulsed laser deposition at 630 °C and 0.4 mbar of oxygen. The growth was monitored in real time by reflection high-energy electron diffraction (RHEED). After deposition the samples were annealed *in situ* for 30 min at 500 °C and 300 mbar of oxygen.

Figure 1(a) shows typical RHEED oscillations of the specular spot intensity indicating layer-by-layer growth of the films. The high surface quality was evidenced by the streaked Bragg reflections observed in the RHEED pattern obtained after growth as shown in Fig. 1(b), and confirmed by atomic

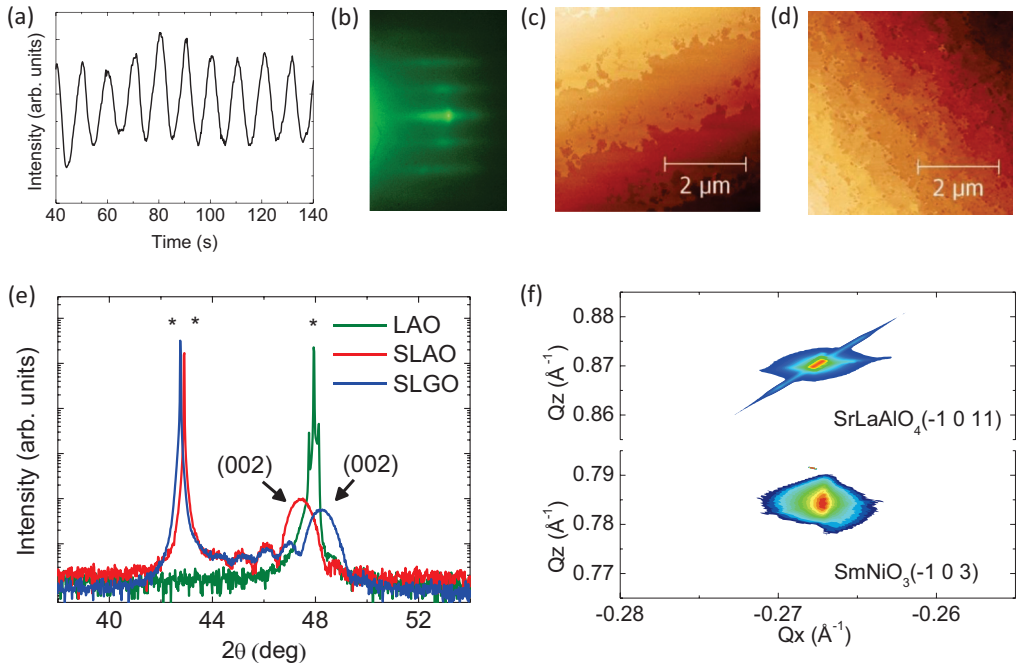

FIG. 1. (Color online) (a) RHEED specular spot intensity observed during growth of a 15-u.c. $SmNiO_3$ thin film on a SLGO substrate, (b) RHEED pattern obtained after deposition. (c) and (d) atomic force microscopy topographic image of 15-u.c. thin films grown on SLAO and SLGO substrates, respectively. (e) X-ray diffraction spectra of 25-u.c. thin films grown on SLAO (red), LAO (green), and SLGO (blue) substrates. (f) Reciprocal space map of a 60-u.c. thin film of $SmNiO_3$ grown on SLAO.

force microscopy; see Figs. 1(c) and 1(d). The sole presence of (0 0 L) peaks in the x-ray diffraction spectra shown in Fig. 1(e) confirmed the films' epitaxial quality, with an out-of-plane lattice constant of 3.829 and 3.754 Å for films on SLAO and SLGO, respectively. For the sample grown on LAO, only the substrate peaks were visible due to the very close lattice match between SNO and LAO. The presence of Laue fringes attested the coherent crystal structure existing over the whole thickness. Reciprocal space maps of samples up to 60 u.c. in thickness indicated that the films were fully strained on the substrates [see an example in Fig. 1(f)].

Figures 2(a) and 2(b) show the resistivity (ρ) and its derivative [$-d\log(\rho)/dT$] as a function of temperature for 25-u.c. films grown on different substrates. The measurements were taken upon cooling down the samples, and no hysteresis was observed when warming up. The resistivity of the film

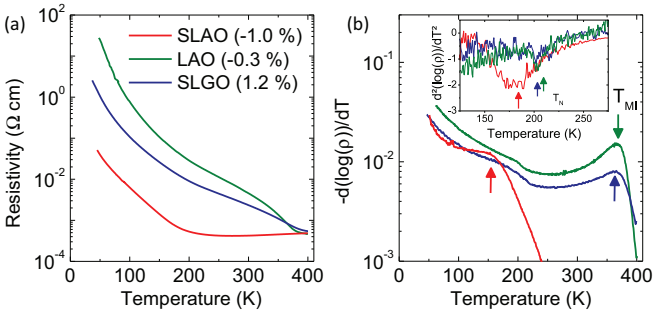

FIG. 2. (Color online) (a) Resistivity and (b) its derivative as a function of temperature for 25-u.c.-thick films grown on SLAO (red), LAO (green), and SLGO (blue) substrates.

grown on LAO shows an inflection point just below 400 K, as for bulk SNO. Between 400 and 50 K, the resistivity is enhanced by five orders of magnitude, an increase even larger than in bulk samples.[22] Here we choose to identify T_{MI} with the peak observed in the [$-d\log(\rho)/dT$] temperature dependence [Fig. 2(b)]. Using this criterion the transition occurs at $T_{MI} = 370$ K for the film grown on LAO, which is close to the reported bulk values. Interestingly, a kink is observed at 205 K [see Fig. 2(b)]. This anomaly is associated with the Néel temperature T_N and the obtained value is close to the bulk $T_N = 225$ K.[23] Thus, SNO thin films on LAO are of high structural quality with almost bulklike physical properties.

We now turn our attention to the films subject to about 1% compressive or tensile strain. While for the latter, T_{MI} is weakly modified ($T_{MI} = 365$ K), for the former it is reduced by over 200 K, occurring at $T_{MI} = 155$ K. The influence of epitaxial strain on the metal-insulator transition is thus strongly asymmetric. Much smaller changes are observed in the Néel temperature for SLAO and SLGO, i.e., $T_N = 185$ K and $T_N = 200$ K, respectively [see inset of Fig. 2(b)]. Note that the different behavior of T_N and T_{MI} with strain suggests a different origin for the magnetic and metal-insulator transition.

To gain insight into the electronic structure and orbital occupancy in our films, we performed x-ray absorption spectroscopy (XAS) experiments at the Ni $L_{3,2}$ edges at the PM3 beamline of the Helmholtz Zentrum Berlin. Absorption spectra (β) were obtained using the total electron yield (TEY) detection mode. To characterize the ground state of each film, the measurements were carried out at 120 K, well into the insulating state. We thus exclude that visible changes in the measured spectra reflect the transition from an insulating to a

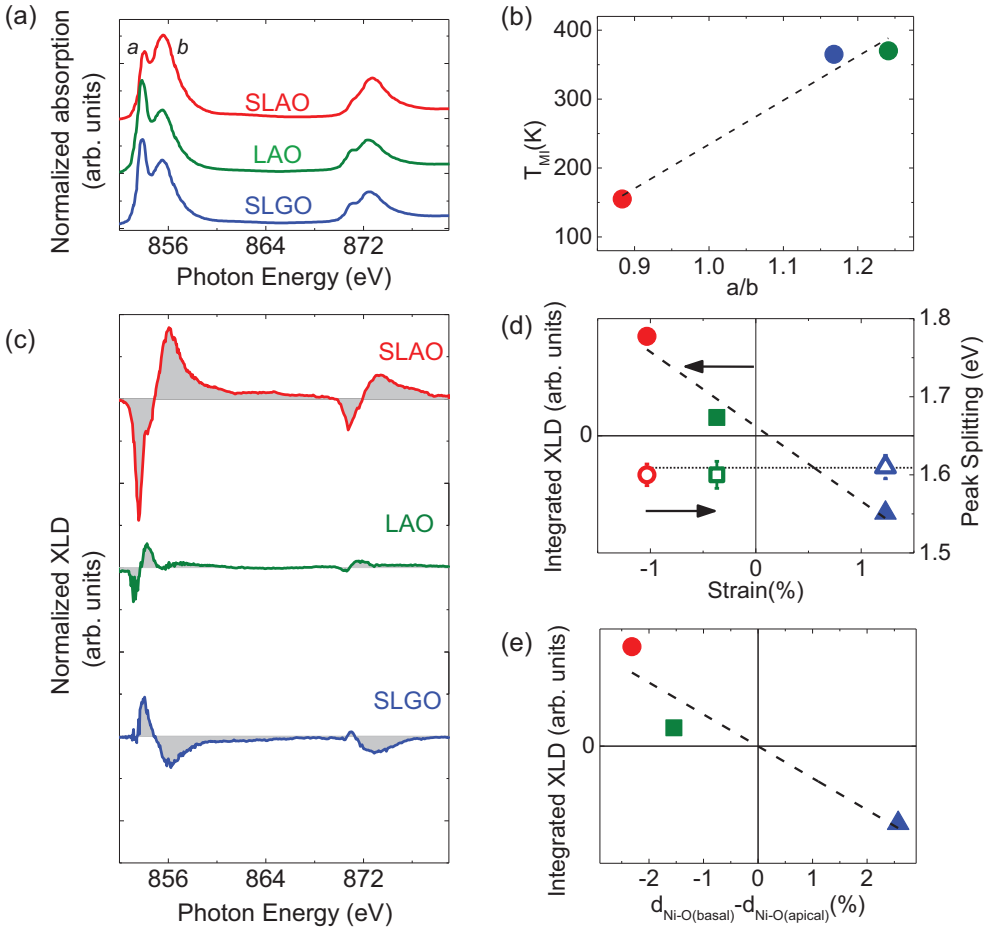

FIG. 3. (Color online) (a) Normalized x-ray absorption spectra and (c) linear dichroism for 25-u.c.-thick samples grown on SLAO (red), LAO (green), and SLGO (blue) substrates. (b) Metal-insulator transition temperature as a function of the a/b peak intensity ratio. Integrated linear dichroism as a function of (d) strain and (e) difference between Ni-O basal and apical distance. Dashed lines are linear fits to the data. Closed symbols correspond to samples grown on different substrates: SLAO (red circles), LAO (green squares), and SLGO (blue triangles). (d) In open symbols, energy peak splitting between a and b features at the Ni-L_3 edge.

metallic state. In Fig. 3(a) we present the Ni-L edge absorption spectra for 25-u.c films obtained in normal incidence with horizontal linearly polarized light. The spectral shape is similar for all films and resembles that obtained in the RNiO$_3$ family in the insulating state, with both L_2 and L_3 peaks showing a splitting into two components, labeled a and b.[24,25] We observe that the three spectra present a different intensity ratio between the a and b features. In the XAS spectra of the RNiO$_3$ family, the a/b ratio decreases upon increasing the size of the R cation, concomitant with the decrease of T_{MI}.[24] Interestingly, we observe a similar effect [cf. Fig. 3(b)], but in this case, it is driven by epitaxial strain rather than by steric effects. The a-b energy splitting was obtained as the difference of the peak positions after performing a multiple peak Gaussian fit of the L_3 edge. Importantly, although the relative intensity of the a and b features varies with strain, their relative positions in energy are independent of strain as shown in open symbols in Fig. 3(d). This a-b energy splitting is related to the charge-transfer energy Δ[21] and we thus conclude that Δ does not depend on strain, and furthermore is not the main parameter driving the observed changes in T_{MI}. This is consistent with the fact that changes in T_{MI} and T_N induced by chemical or hydrostatic pressure were well described with constant values of Δ.[26,27]

The in-plane and out-of-plane orbital occupancy at the Ni sites can be probed by collecting two absorption spectra with linearly polarized light with the light polarization parallel (β^{ab}) and perpendicular to the plane of the sample (β^{c}). The associated x-ray linear dichroism (XLD), i.e., β^{ab}–β^{c}, as well as its integrated intensity, provides information about the preferred orbital occupation.[28–30] In strained nickelate films it is expected that the strained-induced distortion will remove the degeneracy of the two $3d$-e_g orbitals, i.e., $d_{x^2-y^2}$ and $d_{z^2-r^2}$, present in a perfect Ni-O$_6$ octahedron. When compressive epitaxial strain is imposed, the in-plane (out-of-plane) Ni-O distances are reduced (augmented) and consequently the energy of the $d_{z^2-r^2}$ orbital is reduced with respect to the $d_{x^2-y^2}$. The opposite effect is expected from tensile strain. In Ni^{3+} with nominal configuration $t_{2g}{}^6e_g{}^1$ the partially filled e_g band will thus present a preferred orbital polarization. This view, which successfully describes the behavior of the single e_g electron of Mn^{3+} in the related system LaMnO$_3$,[28] however, fails to describe some nickelates.[31] To investigate this issue we have measured the XLD spectra of our films

[Fig. 3(c)]. For the sample on SLAO the XLD presents a large positive contribution on the high-energy side of the $L_{2,3}$ peaks, indicating preferential occupation of the $d_{z^2-r^2}$ orbital.[31] For the film grown on LAO similar features are observed, albeit with much lower intensity. The opposite is observed for SLGO, corresponding to a preferential electron occupation of the $d_{x^2-y^2}$ orbital.

In order to understand how structural changes affect the orbital polarization, T_{MI}, and the overall electronic structure of SNO, we have performed electronic structure calculations, taking into account the different strain states imposed by substrates. We carried out calculations with the Vienna *ab initio* simulation package (VASP)[32–34] with projector-augmented wave pseudopotentials.[35] We used the Heyd-Scuseria-Ernzerhof (HSE) hybrid functional[36,37] and performed the atomic relaxations within the unit cells with the experimentally determined lattice parameters (the results of the structural relaxations are summarized in Table I). The ion positions were relaxed for all considered magnetic configurations until the Hellmann-Feynman forces were smaller than 0.04 eV/Å. Due to the low magnetic ordering temperature of the spins of the rare-earth cations[38] we did not consider them and treated the f shells of Sm in the core. Brillouin-zone integrations were performed with a Gaussian smearing of 0.05 eV over a $2 \times 4 \times 2$ Monkhorst-Pack k-point mesh[39] centered at Γ, with a 500-eV plane-wave cutoff. An 80-atomic unit cell was used for all calculations. This unit cell is necessary to properly describe the 20-atomic $GdFeO_3$-type orthorhombic crystallographic unit cell, with the superimposed $2 \times 1 \times 2$ magnetic structure.[38,40] No symmetry constraints were imposed, allowing possible charge and/or orbital ordering in the ground state. To take into account the magnetic ground state of the system we considered ferromagnetic as well as collinear antiferromagnetic structures of S (AFM-S) and T types (AFM-T). In these antiferromagnetic configurations the Ni spins form ferromagnetic zigzag chains within the ab plane, but with different stacking of the zigzags along the c axis (see Ref. 14). In the AFM-S structure the zigzag spin chains point in the same direction for all the ab planes [Fig. 4(a)], whereas for AFM-T ordering the direction of zigzags alternates for adjacent ab planes [Fig. 4(b)]. Adjacent zigzag chains are always coupled antiferromagnetically in the same ab plane.

TABLE I. Theoretical structural parameters for $SmNiO_3$ epitaxially strained on different substrates. Space group was found to be $P2_1/c$. Fractional atomic positions are given in monoclinic crystallographic setting of tetragonal cells with out-of-plane periods 3.829, 3.826, and 3.754 Å for substrates $SrLaAlO_4$, $LaAlO_3$, and $SrLaGaO_4$, correspondingly.

Lattice parameters	$SrLaAlO_4$	$LaAlO_3$	$SrLaGaO_4$
$a = b$ (Å)	5.3132	5.34856	5.43482
c (Å)	9.32068	9.33555	9.26862
β (deg)	124.75	124.95	125.90
Atom, Wyckoff position, and fractional coordinates			
Sm (4e), x	0.26259	0.26258	0.26084
y	0.44904	0.44802	0.44485
z	0.24994	0.25000	0.25011
Ni1 (2d), x, y, z	0.5, 0, 0.5	0.5, 0, 0.5	0.5, 0, 0.5
Ni2 (2a), x, y, z	0, 0, 0	0, 0, 0	0, 0, 0
O1 (4e), x	0.15286	0.15117	0.14890
y	0.01522	0.01747	0.02253
z	0.23830	0.23840	0.24019
O2 (4e), x	0.32850	0.32819	0.32641
y	0.19912	0.19875	0.19709
z	0.04693	0.04723	0.04674
O3 (4e), x	0.75703	0.75664	0.75789
y	0.28439	0.28375	0.28233
z	−0.04653	−0.04732	−0.04784

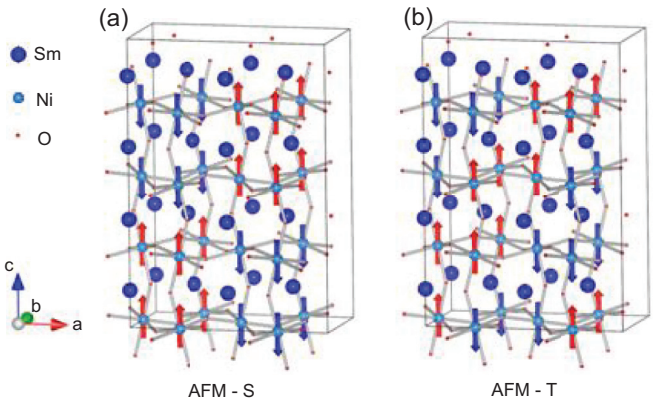

FIG. 4. (Color online) Schemes illustrating relative spin antiferromagnetic arrangements on Ni atoms in (a) AFM-S and (b) AFM-T ordering.

Presented in Table II is the total energy difference (in eV per Ni atom) for ferromagnetic (FM) or AFM-S configurations with respect to the AFM-T ordering. We have found that in all cases the AFM-T corresponds to the ground state, consistent with experimental observations.[23] Therefore, in all further analysis we use the AFM-T structure. We note that the HSE hybrid functional was already applied by Gou *et al.* to describe the lattice vibrations in $LaNiO_3$.[41] Our calculations using HSE show that this functional provides the best description of the magnetic structure in $RNiO_3$, in contrast to our (and recently published[42]) GGA + U calculations, as well as dynamical mean field theory results[43] that found a ferromagnetic (FM) ground state.

In agreement with previous theoretical studies of $RNiO_3$,[42,43] we found that in the ground state there are two inequivalent Ni positions: the Ni1 site with high spin and magnetic moment of the order of 1.5 μ_B and the Ni2 site with zero magnetic moment. In Table III we present the Ni-O distances calculated for both Ni positions as well as the Ni1-O-Ni2 bond angle θ. The oxygen cage around the

TABLE II. Total energy difference (in eV per Ni atom) for ferromagnetic (FM) or antiferromagnetic S-type (AFM-S) configurations with respect to the AFM-T ordering.

Substrate	E(FM)–E(AFM-T)	E(AFM-S)–E(AFM-T)
$SrLaAlO_4$	0.0398	0.0009
$LaAlO_3$	0.0032	0.0607
$SrLaGaO_4$	0.0038	0.0504

TABLE III. Theoretical structural parameters for $SmNiO_3$ epitaxially strained on different substrates. The in-plane parameters are given in the first two rows and the out-of-plane parameter in the third one for each substrate. The Ni1-O-Ni2 bond angle (θ), and the Ni-O distance [d(Ni-O)] are shown. The angle φ is defined as $\varphi = (180–\theta)/2$, and d_{av} is the average distance.

Substrate	θ (deg)	d(Ni1-O) (Å)	d(Ni2-O), Å	φ (deg)	$\cos(\varphi)/d_{av}^{3.5}$
	151.61	2.008	1.867	14.194	0.09576
$SrLaAlO_4$	150.96	2.010	1.871		
	152.86	2.056	1.882		
	151.67	2.025	1.876	14.165	0.09356
$LaAlO_3$	150.85	2.028	1.880		
	152.01	2.058	1.885		
	152.28	2.066	1.892		
$SrLaGaO_4$	151.13	2.071	1.897		
	149.50	2.016	1.875	15.248	0.09398

Ni1 site is strongly anisotropic and forms a nearly square bipyramidal crystal field around it, whereas the surrounding of the Ni2 site is almost that of a regular octahedron (see Tables I and III). The oxygen p orbitals therefore form strong σ bonds towards Ni2, but with an angle different from 180° towards the Ni1 sites. We also find that the charge integrated around both Ni sites nearly corresponds to a d^8 configuration and is not dependent on the substrate.[43]

A first consistency check between theoretical and experimental results can be carried out at this point, since the deformation of the octahedral sites is related to the splitting of the $d_{z^2-r^2}$ and $d_{x^2-y^2}$ orbitals. Figures 3(d) and 3(e) display the integrated XLD signal as a function of the strain and the calculated distortion of the Ni1-O_6 oxygen octahedral (see Table III), respectively. This distortion is determined as the difference between the average Ni-O distance in the basal (ab) plane and the average distance with the apical (c direction) oxygen taken from Table III. The changes observed in Figs. 3(d) and 3(e) are very similar. Thus, in addition to yielding the proper magnetic ground state, our calculations correctly predict the atomic positions in strained SNO films. Interestingly, we observe that strain variations of 1% lead to 2% changes in the Ni1-O distances. This result is a consequence of the existence of two inequivalent Ni sites where only the Ni1-O_6 octahedra are strongly distorted.

The calculated density of states shown in Fig. 5(a) based on HSE also correctly describes this experimental observation. In the deformed octahedra of the Ni1 site the degenerate e_g states split into $d_{z^2-r^2}$ and $d_{x^2-y^2}$ orbitals. This splitting is proportional to the in-plane deformation. The $d_{z^2-r^2}$ peak observed below and above the Fermi level is lower in energy than the $d_{x^2-y^2}$ one for the film on the SLAO substrate, whereas the situation is the opposite for the case of the SLGO substrate. On LAO, due to the low strain, the splitting is small compared

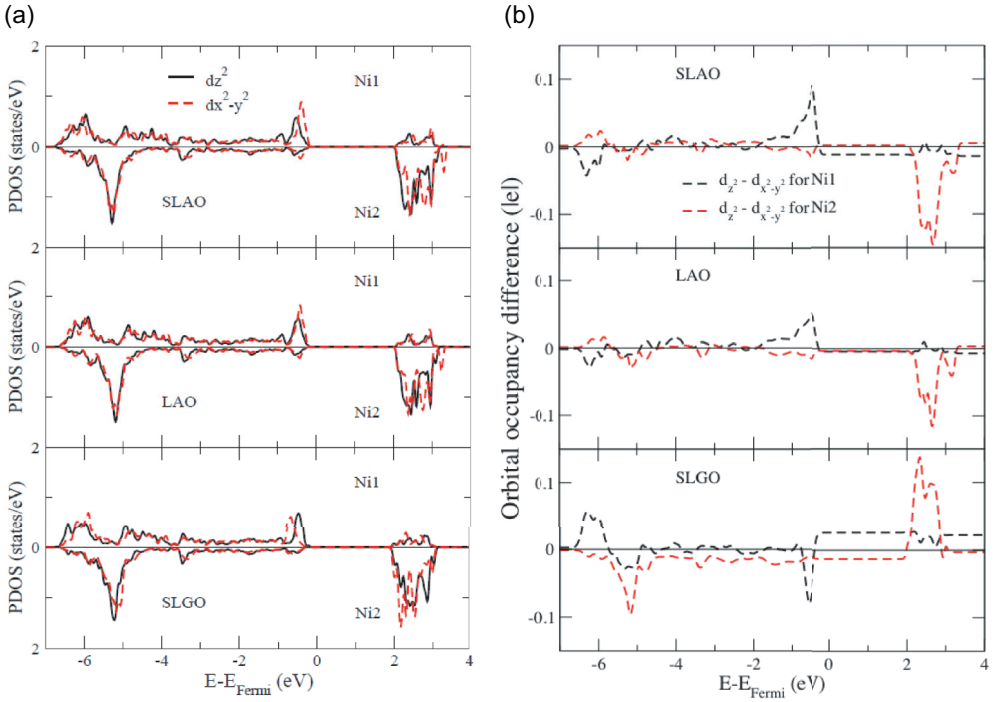

FIG. 5. (Color online) (a) Density of e_g states calculated for both sublattices of Ni atoms in a $SmNiO_3$ thin film: Top (SLAO), middle (LAO), and bottom (SLGO). (b) Difference in orbital occupancy (in elementary charge units) of e_g-like d states of Ni.

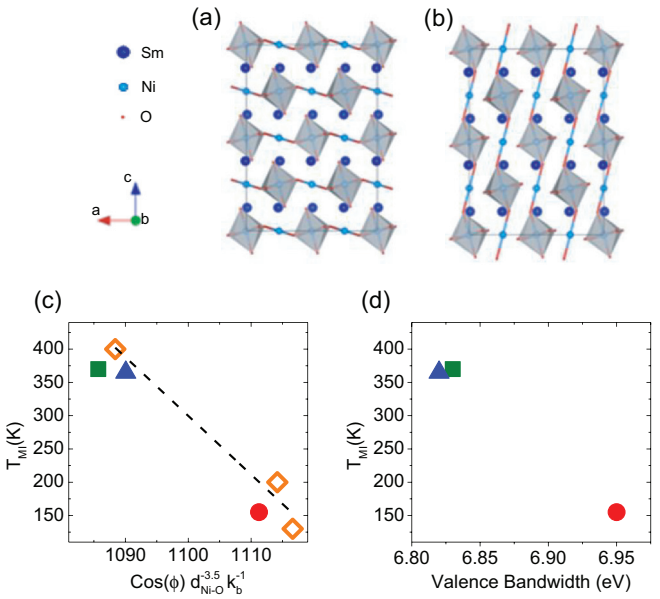

FIG. 6. (Color online) Schemes illustrating the shortest Ni1-O-Ni2 bonds for the case of (a) SLAO and LAO and (b) SLGO substrates. The Ni2 atoms are in the center of the depicted polyhedra, and for the Ni1 atoms only the shortest distance is plotted. (c) Metal-to-insulator transition temperature as a function of $\cos(\varphi)/d_{\mathrm{Ni-O}}^{3.5}$ and (d) as a function of the valence bandwidth obtained from band structure calculations. Closed symbols correspond to samples grown on different substrates: SLAO (red circles), LAO (green squares), and SLGO (blue triangles). Open symbols correspond to structural and T_{MI} data corresponding to bulk $SmNiO_3$, $NdNiO_3$, and $PrNiO_3$ taken from Refs. 5,22,44.

to the situation on SLAO. In Fig. 5(b) we show the difference between $d_{z^2-r^2}$ and $d_{x^2-y^2}$ density of states to emphasize the possibility of tuning orbital occupations with different substrates. The fact that orbital polarization is observed in a system where the charge integrated around both Ni sites nearly corresponds to a d^8 configuration is not surprising if one takes into account the strong Ni-O hybridization in SNO.

In order to relate the experimentally observed trend in the T_{MI} with structural changes on different substrates, we adopted the scheme described in Ref. 26 in the following form:

$$k_b T_{\mathrm{MI}} = \Delta - A\frac{\cos(\varphi)}{d_{\mathrm{Ni-O}}^{3.5}}. \qquad (1)$$

Here Δ is the charge-transfer energy [which from Fig. 3(b) we assume to be constant with strain], the bare bandwidth W_b is proportional to $\cos(\varphi)/d_{\mathrm{Ni-O}}^{3.5}$, A is a proportionality constant,[26] $\varphi = (180–\theta)/2$ is the tilting angle (in degrees) of the NiO_6 octahedra, and θ is the Ni-O-Ni superexchange angle. In Fig. 6(c) we present in open symbols the experimental values of T_{MI} as a function of $\cos(\varphi)/d_{\mathrm{Ni-O}}^{3.5}$ for three bulk nickelates with R = Pr, Nd, and Sm.[5,22,44] The maximum Ni-O-Ni angle and the average between the two shortest $d_{\mathrm{Ni1-O}}$ and $d_{\mathrm{Ni2-O}}$ distances corresponding to the widest bare bandwidth are taken for each material. A linear fit yields values for the constants used in Eq. (1), i.e., $\Delta = 0.86$ eV and $A = 8.83$ eV Å$^{3.5}$. The obtained charge-transfer energy is consistent with previously calculated values ($\sim$1 eV).[45] In the same figure we plot with closed symbols the experimental values of T_{MI} vs $\cos(\varphi)/d_{\mathrm{Ni-O}}^{3.5}$ for our films, where the angles and bond lengths were determined by first-principles calculations (see Table III). The trend is very similar to that of bulk samples. Note that the widest bandwidth corresponds to the bonds lying in ab plane for the case of SLAO and LAO substrates whereas for the case of SLGO this corresponds to the out-of-plane bonds. The Ni-O-Ni bonds corresponding to the direction of maximum bandwidth are shown in Fig. 6(a) for SLAO and LAO and in Fig. 6(b) for the case of SLGO. Finally, we also plot T_{MI} as a function of the valence bandwidth calculated from first principles in Fig. 6(c). Again, a systematic linear dependence is found. We thus conclude that, based on our theoretical description of the system, the bandwidth changes in strained thin films are responsible for the changes in T_{MI}.

In summary, we have applied epitaxial strain to tune the orbital occupancy and the metal-insulator transition temperature in $SmNiO_3$ thin films. *Ab initio* calculations using the Heyd-Scuseria-Ernzerhof functional and constrained by the experimentally observed lattice periodicities were also performed. The calculations correctly describe the insulating and antiferromagnetic ground state of the system, as well as the preferential orbital polarization observed by x-ray linear dichroism experiments. Comparison between transport, spectroscopy, and theoretical data shows that the observed strain-induced variation in the metal-insulator transition temperature is a consequence of changes in the electron bandwidth rather than in the charge-transfer energy or in the density of structural defects as alternatively proposed. Our work is extendable to other nickelates and emphasizes the relevance of the HSE functional to discriminate between nearly degenerate ground states and to disentangle the role of individual structural parameters in strongly correlated oxides.

We acknowledge financial support from the European Research Council (ERC Advanced Grant FEMMES, No. 267579). This work was partially supported by the Young Investigators Group Programme of the Helmholtz Association, Germany, Contract No. VH-NG-409. We gratefully acknowledge the support of Jülich Supercomputing Centre and JARA-HPC from RWTH Aachen University under Project jara0041. Spectroscopy experiments using the ALICE end station were financed through BMBF 05K10PC1 project. We thank Helmholtz Zentrum Berlin for the allocation of synchrotron radiation beam time and for providing financial support. Transport measurements have been performed thanks to "NOVATECS" C'Nano IdF Project n°IF-08-1453/R.

[1] P. Lacorre, J. B. Torrance, J. Pannetier, A. I. Nazzal, P. W. Wang, and T. C. Huang, J. Solid State Chem. **91**, 225 (1991).
[2] J. B. Torrance, P. Lacorre, A. I. Nazzal, E. J. Ansaldo, and C. Niedermayer, Phys. Rev. B **45**, 8209 (1992).
[3] M. L. Medarde, J. Phys.: Condens. Matter **9**, 1679 (1997).
[4] G. Catalan, Phase Transitions **81**, 729 (2008).
[5] M. Medarde, M. T. Fernández-Díaz, and P. Lacorre, Phys. Rev. B **78**, 212101 (2008).

[6]M. Medarde, C. Dallera, M. Grioni, B. Delley, F. Vernay, J. Mesot, M. Sikora, J. A. Alonso, and M. J. Martínez-Lope, Phys. Rev. B **80**, 245105 (2009).
[7]J. H. Haeni, P. Irvin, W. Chang, R. Uecker, P. Reiche, Y. L. Li, S. Choudhury, W. Tian, M. E. Hawley, B. Craigo, A. K. Tagantsev, X. Q. Pan, S. K. Streiffer, L. Q. Chen, S. W. Kirchoefer, J. Levy, and D. G. Schlom, Nature (London) **430**, 758 (2004).
[8]J. H. Lee, L. Fang, E. Vlahos, X. Ke, Y. W. Jung, L. F. Kourkoutis, J.-W. Kim, P. J. Ryan, T. Heeg, M. Roeckerath, V. Goian, M. Bernhagen, R. Uecker, P. C. Hammel, K. M. Rabe, S. Kamba, J. Schubert, J. W. Freeland, D. A. Muller, C. J. Fennie *et al*., Nature (London) **466**, 954 (2010).
[9]M. Ležaić and N. A. Spaldin, Phys. Rev. B **83**, 024410 (2011).
[10]D. Sando, A. Agbelele, D. Rahmedov, J. Liu, P. Rovillain, C. Toulouse, I. C. Infante, A. P. Pyatakov, S. Fusil, E. Jacquet, C. Carrétéro, C. Deranlot, S. Lisenkov, D. Wang, J.-M. Le Breton, M. Cazayous, A. Sacuto, J. Juraszek, A. K. Zvezdin, L. Bellaiche *et al*., Nat. Mater. **12**, 641 (2013).
[11]A. Boris, Y. Matiks, E. Benckiser, A. Frano, P. Popovich, V. Hinkov, P. Wochner, M. Castro-Colin, E. Detemple, V. K. Malik, C. Bernhard, T. Prokscha, A. Suter, Z. Salman, E. Morenzoni, G. Cristiani, H.-U. Habermeier, and B. Keimer, Science **332**, 937 (2011).
[12]J. Chaloupka and G. Khaliullin, Phys. Rev. Lett. **100**, 016404 (2008).
[13]K.-Y. Yang, W. Zhu, D. Xiao, S. Okamoto, Z. Wang, and Y. Ran, Phys. Rev. B **84**, 201104 (2011).
[14]G. Giovannetti, S. Kumar, D. Khomskii, S. Picozzi, and J. van den Brink, Phys. Rev. Lett. **103**, 156401 (2009).
[15]R. Jaramillo, F. Schoofs, S. D. Ha, and S. Ramanathan, J. Mater. Chem. C **1**, 2455 (2013).
[16]M. Imada, A. Fujimori, and Y. Tokura, Rev. Mod. Phys. **70**, 1039 (1998).
[17]J.-G. Cheng, J.-S. Zhou, J. B. Goodenough, J. A. Alonso, and M. Martinez-Lope, Phys. Rev. B **82**, 085107 (2010).
[18]A. Tiwari, C. Jin, and J. Narayan, Appl. Phys. Lett. **80**, 4039 (2002).
[19]R. Scherwitzl, P. Zubko, I. G. Lezama, S. Ono, A. F. Morpurgo, G. Catalan, and J.-M. Triscone, Adv. Mater. **22**, 5517 (2010).
[20]J. Liu, M. Kareev, B. Gray, J. W. Kim, P. Ryan, B. Dabrowski, J. W. Freeland, and J. Chakhalian, Appl. Phys. Lett. **96**, 233110 (2010).
[21]D. Meyers, S. Middey, M. Kareev, M. van Veenendaal, E. J. Moon, B. A. Gray, J. W. Freeland, and J. Chakhalian, arXiv:1304.1751.
[22]J. Pérez-Cacho, J. Blasco, J. García, M. Castro, and J. Stankiewicz, J. Phys.: Condens. Matter **11**, 405 (1999).
[23]J. Rodríguez-Carvajal, S. Rosenkranz, M. Medarde, P. Lacorre, M. T. Fernandez-Díaz, F. Fauth, and V. Trounov, Phys. Rev. B **57**, 456 (1998).
[24]C. Piamonteze, F. M. F. de Groot, H. C. N. Tolentino, A. Y. Ramos, N. E. Massa, J. A. Alonso, and M. Martínez-Lope, Phys. Rev. B **71**, 020406(R) (2005).
[25]V. Scagnoli, U. Staub, A. M. Mulders, M. Janousch, G. I. Meijer, G. Hammerl, J. M. Tonnerre, and N. Stojic, Phys. Rev. B **73**, 100409(R) (2006).
[26]M. Medarde, P. Lacorre, K. Conder, F. Fauth, and A. Furrer, Phys. Rev. Lett. **80**, 2397 (1998).
[27]J.-S. Zhou, J. B. Goodenough, and B. Dabrowski, Phys. Rev. Lett. **94**, 226602 (2005).
[28]Y. Tokura and N. Nagaosa, Science **288**, 462 (2000).
[29]F. Yildiz, F. Luo, C. Tieg, R. M. Abrudan, X. L. Fu, A. Winkelmann, M. Przybylski, and J. Kirschner, Phys. Rev. Lett. **100**, 037205 (2008).
[30]J. Garcia-Barriocanal, J. C. Cezar, F. Y. Bruno, P. Thakur, N. B. Brookes, C. Utfeld, A. Rivera-Calzada, S. R. Giblin, J. W. Taylor, J. A. Duffy, S. B. Dugdale, T. Nakamura, K. Kodama, C. Leon, S. Okamoto, and J. Santamaria, Nat. Commun. **1**, 82 (2010).
[31]J. Chakhalian, J. M. Rondinelli, J. Liu, B. A. Gray, M. Kareev, E. J. Moon, N. Prasai, J. L. Cohn, M. Varela, I. C. Tung, M. J. Bedzyk, S. G. Altendorf, F. Strigari, B. Dabrowski, L. H. Tjeng, P. J. Ryan, and J. W. Freeland, Phys. Rev. Lett. **107**, 116805 (2011).
[32]G. Kresse and J. Furthmüller, Phys. Rev. B **54**, 11169 (1996).
[33]G. Kresse and D. Joubert, Phys. Rev. B **59**, 1758 (1999).
[34]G. Kresse and J. Hafner, Phys. Rev. B **47**, 558 (1993).
[35]P. E. Blöchl, Phys. Rev. B **50**, 17953 (1994).
[36]J. Heyd, G. E. Scuseria, and M. Ernzerhof, J. Chem. Phys. **118**, 8207 (2003).
[37]J. Heyd, G. E. Scuseria, and M. Ernzerhof, J. Chem. Phys. **124**, 219906 (2006).
[38]M. T. Fernández-Díaz, J. A. Alonso, M. J. Martínez-Lope, M. T. Casais, and J. L. García-Muñoz, Phys. Rev. B **64**, 144417 (2001).
[39]H. J. Monkhorst and J. D. Pack, Phys. Rev. B **13**, 5188 (1976).
[40]J. A. Alonso, J. L. García-Muñoz, M. T. Fernández-Díaz, M. A. G. Aranda, M. J. Martínez-Lope, and M. T. Casais, Phys. Rev. Lett. **82**, 3871 (1999).
[41]G. Gou, I. Grinberg, A. M. Rappe, and J. M. Rondinelli, Phys. Rev. B **84**, 144101 (2011).
[42]S. Prosandeev, L. Bellaiche, and J. Íñiguez, Phys. Rev. B **85**, 214431 (2012).
[43]H. Park, A. J. Millis, and C. A. Marianetti, Phys. Rev. Lett. **109**, 156402 (2012).
[44]J. L. García-Muñoz, J. Rodríguez-Carvajal, P. Lacorre, and J. B. Torrance, Phys. Rev. B **46**, 4414 (1992).
[45]T. Mizokawa, A. Fujimori, T. Arima, Y. Tokura, N. Mōri, and J. Akimitsu, Phys. Rev. B **52**, 13865 (1995).